RSC Advances

Microfluidic-assisted cyclic mechanical stimulation affects cellular membrane integrity in a human muscle dystrophy in vitro model.

SCHOLARONE™
Manuscripts

Microfluidic-assisted cyclic mechanical stimulation affects cellular membrane integrity in a human muscle dystrophy *in vitro* model

Michielin F. [1,2], Serena E. [1,2], Pavan P. [1,3], and Elvassore N. [1,2,]*

[1] Department of Industrial Engineering (DII), University of Padova, Padova, Italy.

[2] Venetian Institute of Molecular Medicine (VIMM), Padova, Italy.

[3] Centre for Mechanics of Biological Materials (CMBM), University of Padova, Padova, Italy.

Running title: Stretch-induced membrane

Keywords: stretch, microfluidic, myotubes, membrane integrity.

*Corresponding author address:
Dipartimento di Ingegneria Industriale DII,
University of Padova,
Via Marzolo, 9. 35131 Padova, Padova, Italy,
E-mail: nicola.elvassore@unipd.it,
Tel.: +39 049 8275469, Fax: +39 049 8275461

Abstract

Cyclic mechanical stimulation has been found to deeply affect cell behavior in terms of cytoskeleton remodeling, signaling pathways alteration and differential gene expression in several diseases. In Duchenne Muscular Dystrophy (DMD), the lack of protein Dystrophin, which plays a structural and regulatory role in preserving membrane integrity and homeostasis, mechanical stress seems to enhance the pathogenesis of muscle fibers, as resulted in many studies on mdx, a DMD mouse model.

In this study we aimed at investigating if the lack of Dystrophin results in impairment of membrane integrity after prolonged cyclic mechanical stimulations in a human *in vitro* model. We developed an *ad hoc* microfluidic-based cell-stretching device in order to apply defined external stimuli, in terms of both frequency and intensity, to primary myoblast and myotube cell cultures. Computational modeling supported the design of the device, in order to estimate the mechanical state induced on the cells. Both static and cyclic (1 Hz) mechanical stretch for 2 h on myoblasts show a frequency-dependent cytoskeletal actin filaments remodeling along the direction of minimum strain. On the other hand, an over physiological stretch stimulation (20% strain) show localized membrane impermeant marker uptake due to loss of membrane integrity. Interestingly, human myotubes resulted more sensitive to mechanical stretch than myoblasts.

Thanks to the developed technology we were able to investigate how cyclic stretch affects membrane permeability of both healthy and dystrophic myotubes. The results show that DMD myotubes have a higher stretch-induced membrane permeability compared to healthy myotubes, both subjected to 90 min cyclic strain of 15%. Interestingly, the same effect was not observed after only 45 min of the same cyclic strain. We also investigated the implication of increased stretch-dependent membrane permeability in the activation of the calcium dependent protease Calpain-2, which is recognized to be aberrantly expressed in dystrophic myotubes.

This microfluidic approach allows accurate and temporally defined mechanical stimulations at single or subcellular level. Moreover, it could be used to study early pathologic events and potential therapeutic approaches on skeletal muscle disease *in vitro* model subjected to stress conditions normally experienced by muscle fibers *in vivo*.

1. Introduction

Mechanical stress plays a crucial role in the investigation of new physiological and pathological responses to cell culture microenvironment. It is recognized that active deformation promotes cellular growth and survival, influences metabolic processes and gene expression, and governs tissue architecture in various cell types[1,2,3,4,5]. Muscle cells are particularly responsive to mechanical forces; indeed, expression of skeletal muscle specific genes and skeletal muscle functional maturation, including sarcomeric structural organization and contractile apparatus development, can be modulated by applying an external mechanical stress[2,6]. The myofiber forms the functional unit of skeletal muscle *in vivo*, in which a regular array of contractile units (sarcomeres) comprised of thin actin filaments and thick myosin filaments that, along with additional structural and regulatory proteins, allow response to mechanical stress[7]. The peripheral myofibrils are connected to the sarcolemma along the Z-disks via interactions with sub-sarcolemmal protein complexes called costameres. These structures transmit contractile forces from sarcomeres of one myofiber to another, which prevents sarcolemma ruptures by synchronizing contraction of myofibers within the muscle. The integrity of this protein complex is crucial for the contracting myofiber to withstand the mechanical stress generated by sarcomeres and to prevent its fragile sarcolemma from contraction-induced injuries[7]. Failure to attach properly results in sarcolemmal disruption, which is the predominant underlying cause of several forms of muscular dystrophies. Among them, Duchenne Muscular Dystrophy (DMD) is caused by mutation in gene encoding for protein Dystrophin, which is a large protein and central membrane complex component[8], compromising the mechanical stability of the muscle fiber and/or its sarcolemma. Muscle fibers damage is exacerbated during normal muscle contractions and initiates a lethal cascade of events that can cause death of the myofiber[8] (necrosis) and fibrotic tissue formation[9].

At cellular level, cytoskeletal protein Dystrophin plays a crucial role in the structural maintenance of myofibers membrane integrity, as well as in the regulation of membrane homeostasis[10]. Lack of Dystrophin in mdx mouse, a DMD mouse model, has been shown to cause aberrant mechano-transduction in skeletal muscle fibers[11,12], and mechanical stress seems to deeply affect the disease pathogenesis by triggering intracellular calcium increase, which finally leads to fibers necrosis[13,14].

Many studies recognize an increased stretch-sensible channels activity in mdx muscles, compared to the healthy ones[10,13,15,16,17]. This abnormal activity causes an accumulation of intracellular calcium, $[Ca^{2+}]_i$, which makes the membrane more permeable either through activation of phospholipase A2 or by excessive production of ROS, leading to lipid peroxidation, and enhances membrane permeability. Allen et al. reviewed that a variety of stretch-activated and store-activated

channels have all been shown to function abnormally in dystrophic muscle, although the mechanism by which the absence of Dystrophin triggers abnormal channel activity remains unclear[18]. Conversely, there is broad evidence that muscle fibers from mdx mouse are weaker and more permeable to soluble factors and macromolecules when exposed to cycles of mechanical stimulations. Moreover, eccentric contractions allow soluble cytosolic proteins such as creatine kinase, to leak out of the plasma membrane, whereas extracellular proteins, such as albumin and fibronectin can be detected inside the muscle[18,19]. Experimentally the increased membrane permeability has been repeatedly confirmed by studies in which markers normally membrane impermeant, such as albumin and Evans Blue dye, can be detected inside muscle fibers[18,20], whereas membrane damage was reduced by stretch-activated channel blockers which would have prevented the rise in intracellular calcium $[Ca^{2+}]_i$[21]. These experimental evidences on mdx mice prove that cyclic mechanical stimulation strongly affects the maturation of dystrophic muscle phenotype, suggesting a central role also in humans. However, a human *in vitro* study directed at recapitulating physiological mechanical stress-induced effects on dystrophic skeletal muscle has never been reported so far.

For this reason we aim at developing a human DMD skeletal muscle *in vitro* model in order to investigate the role of cyclic mechanical stress in affecting membrane integrity. Mimicking stress-induced membrane damage *in vitro* requires the development of appropriate technological solutions, which allow tight control of stimulation distinguishing between physiologic and non-physiologic deformation and dynamics. A number of technological solutions have been proposed for stretching cultured cells by using elastic membrane. Beside the most common commercially-available cell-stretching device (Flexcell Corporation) and largely adopted in many works[1,2,22], a number of custom-made solutions have been proposed to perform mechanical stimulations on cell cultures in uniaxial and biaxial directions. For instance, Grossi et al. used a magnetic beads-based assay to mechanically stimulate C2C12 myoblasts under the effect of a magnetic field[23], whereas, Akbari et al. developed two sets of high-throughput single cell stretcher device based on dielectric elastomer micro-actuators to stretch groups of individual cells with various strain levels in a single experiment[24]. However, the accurate control in space and time of mechanical-induced deformations while observing the cellular behavior at single cell level through optical confocal microscopy, are not straightforward. Moreover, the relative large scale of the existing technology hinders to investigate high temporal resolution cell behavior under fast cyclic mechanical stimulations. More sophisticated technological solutions, such as by coupling Myotack sealant and micro-tweezers[25,26], were also proposed for performing single cell mechanical stimulation. However, the intrinsic complexity of these systems make difficult to simultaneously perform multi-parallel experiments

analyzing the mechano-associated single cell response in a high-throughput manner. From this point of view, microfluidic technology ensures tight control of cell culture environment while allowing parallel and multiplexed operation. A number of works have been published to induce precise mechanical stimuli on cultured cells mainly based on the pressurization of microfluidic channels, which drive the deformation of small regions membranes with constant or variable magnitude[27,28,29,30,31,32,33]. Mechanical strain of PDMS membrane can be achieved either by using vacuum systems, which pull the membrane in defined direction while maintaining constant focal plane[30,32,34], or through microfluidic channels pressurization, which induce membrane lift or suction to achieve elongation or compression strain respectively[27,28,29,31]. In the same time, the miniaturization of the system allows high reproducibility of cyclic mechanical stimuli even with high frequencies. The development of these microfluidic devices allowed investigating specific cell responses to external mechanical strain, mainly regarding cytoskeletal remodeling, cell reorientation, protein nuclear translocation and cell differentiation.

In this work we designed an *ad hoc* cell-stretching device, based on the microfluidic technology, in which we integrated a human DMD in vitro model of membrane integrity assay. The developed device allowed applying defined cyclic mechanical deformation on several micro-regions inside the same culture chamber, both in radial and circumferential direction. The intrinsic nano- to micro-liter volume of the system allow achieving frequencies up to 2 Hz in 32 independent observation fields within the same device, with the advantage of having internal not stimulated controls of every single experiment. The elastic membrane surface was properly functionalized for growth and functional differentiation of healthy and DMD human myotubes, whereas microfluidic-driven mechanical stimulation was automatically controlled by an external pneumatic. Computational modeling to fully characterize elastic membrane deformation under application of the internal pressure and to estimate the level of local strains supported the development of the device. These data were adopted in order to accurately calibrate the mechanical bi-component deformation induced on the cells.

Thanks to the developed device we were able to investigate the effect of cyclic physiologic stretch on early pathological events in dystrophic myotubes by using a human DMD *in vitro* model. We investigate the role of cyclic stretch in affecting membrane permeability of both healthy and dystrophic myotubes through the use of a membrane impermeant dye, showing higher membrane permeability in dystrophic myotubes, compared to the healthy ones.

2. Experimental methods

2.1 Cell culture

C2C12 cells were obtained from ATCC bank and cultured in Low-Glucose Dulbecco's Modified Eagle Medium (DMEM) (Sigma-Aldrich), supplemented with 10% Fetal Bovine Serum (FBS) (Life Technologies), and 1% Penicillin–Streptomycin (Life Technologies). Human myoblasts from both healthy and diseased patients were provided by ''Telethon BioBank'' (Telethon Research Service, Istituto Nazionale Neurologico ''Carlo Besta'', Milano, Italy). Myoblasts were expanded in 0.1% gelatin coated Petri dish with proliferative medium: 60% High-Glucose Dulbecco's Modified Eagle's Medium, DMEM, with Glutamax (Life Technologies), 20% M199Medium (Sigma-Aldrich), 20% FBS (Life Technologies), 10 ng/ml EGF (PeproTech, Rocky Hill, NJ), 2 ng/ml β-FGF (PeproTech), 10 ng/ml insulin (insulin from bovine pancreas, Sigma-Aldrich), Penicillin-Streptomycin-Glutamine (Life Technologies). At 80-90% confluence, cells were trypsinized with 0.25% Tripsina-EDTA (Life Technologies) and re-plated either in a new dish or onto stretching devices. Myoblasts were induced to form myotubes in differentiating medium: 98% High-Glucose DMEM, 2% horse serum (Life Technologies), 30 ng/mL insulin, Glutamax, Penicillin-Streptomycin.

2.2 Cell-stretching device fabrication and management

Stretching-devices were fabricated by using standard soft-lithography technique. High resolution-printed photo-mask was photo-lithografically patterned on a silicon wafer by spin-coating SU8-2050 negative photoresist (Microchem, Newton, MA) at 4000 rpm for 30 s to achieve a homogeneous pattern with thickness 50 μm. Silicon wafer was treated with hexamethyldisilazane, HDMS, (Sigma-Aldrich) for 1 h under vacuum. A premixed solution of polydimethylsiloxane, PDMS, pre-polymer and curing agent 10:1 ratio (Dow Corning, Midland, MI) was spun on the silicon wafer at 600 rpm for 1 min and cured at 80°C for 1h. Annular-shaped PDMS blocks were cut and assembled to the elastic membrane to confine cell culture medium. The assembled blocks were cut and peeled off, punched to obtain gas inlet holes and sealed to a glass slide by plasma bonding (Harrick Plasma, Ithaca, NY).

21G stainless steel needles (Small Parts Inc., Logansport, IN) and Tygon micro-tubings (Cole-parmer, Vernon Hills, IL) were used for fluidic connections. Membrane deformation was achieved by gas-pressurization of microfluidic channels; air pressure was accurately controlled through a 0.05 bar resolution pressure regulator (RP1000-8G-02, CKD Corporation, Japan). Stretch frequency was set through an external home-made apparatus equipped with 8 independent automatic electro-valves (M3MAO, CKD Corporation, Japan) controlled by a digital DAQ system,

7

NI USB-6008, (National Instruments, Austin, TX), managed with NI-DAQmx driver and Labview software (National Instruments).

2.3 Structural modeling

Finite Element (FE) Models of different spots were developed in order to estimate the mechanical state induced on the cells. Stress-strain behavior of PDMS was evaluated by uni-axial tensile mechanical tests (Planar Biaxial TestBench® Test System, Bose ElectroForce®, Eden Prairie, MI). The tests were developed at room temperature, adopting a strain rate in the range expected during cell deformation. In the range investigated, the stress-strain response of PDMS was found to be independent of the strain rate. Therefore, an incompressible isotropic hyperelastic constitutive model (of neo-Hookean type) was adopted to describe the mechanical response of PDMS. The constitutive model is defined by the strain energy function:

$$W = \mu(I_1 - 3) + p(J - 1)$$

where I_1 is the first invariant of the right Cauchy-Green strain tensor and J the Jacobian of the deformation. The scalar p is the hydrostatic pressure and the stress-like constitutive parameter μ is the shear modulus of the material at small strains. In uni-axial state the Cauchy stress σ is given by:

$$\sigma = \mu\left(\lambda^2 - 1/\lambda^4\right)$$

where λ is the stretch in the loading direction. The constitutive model was fitted by minimizing the difference between stress experimental data and numerical results and obtaining the value of the constitutive parameter μ for the different composition PDMS. The structural and loading symmetry of different spots was exploited, developing axial-symmetrical models, The nodes at the interface with glass and with adjacent membranes were fixed to simulate the effective boundary conditions. A uniform pressure, with value in the range of experimental tests, was applied in the lower surface of the membranes. Because of the uncompressible behavior of PDMS, hybrid elements (i.e. pressure-displacement) were adopted to avoid locking phenomena. Four node linear axial symmetric elements with uniform size were adopted for the mesh. The mesh density was chosen in order to have results not affected by mesh size changing. According to the elastic behavior assumed for PDMS and the negligible value of inertial forces, the spot deformations were simulated by means of non-linear static analysis, A comparison between numerical results and experimental behavior of the spots was made. At this purpose, experimental values of vertical displacement were obtained by tracking the z-coordinate before and under constant pressurization in the center of the spot with an optical microscope.

2.4 Substrates functionalization and cell seeding

PDMS substrates were coated with 2 $\mu g/cm^2$ bovine fibronectin solution (Sigma-Aldrich). Myoblasts were seeded at 50000 cells/cm^2 density and incubated at 37°C and 5% CO_2 to allow cells attachment on the stretching devices. At 90% confluence, proliferating medium was replaced by differentiation medium, in order to induce myoblasts fusion. The medium was no longer changed for 6 days.

2.5 Stretching experiments and membrane integrity analysis

Cells cultured on microfluidic devices were washed twice with PBS and loaded with buffer solution: 125 mM NaCl, 5 mM KCl, 1 mM Na_3PO_4, 1 mM $MgSO_4$, 20 mM Hepes, 2 mM $CaCl_2$, 5.5 mM Glucose and NaOH to achieve pH 7.4. For membrane integrity assays, cells were also supplemented with 4 μM membrane impermeant marker FM 1-43 (Life Technologies).

Cell culture were stretched at defined frequency for 90 or 45 min and washed twice with PBS or fixed for immunostaining. Images were captured with an optical microscope (Leica Microsystems, Wetzlar, Germany) at 40x magnification. In order to quantify dye uptake in stretched and control myotubes, fluorescence intensity was analyzed on single myotube cytosolic regions, through LAS AF Lite software (Leica Microsystems). Background fluorescence was detected in both stretching and control regions of the device and subtracted to fluorescence intensity of stretched and non-stretched myotubes, respectively. We confined the analysis of stretched myotubes to cells localized in a sub-region of the membrane surface, namely a concentric circle of 300 μm instead of the entire spot of 500 μm, in order to minimize strains variation along the radial coordinate. Data are presented as fluorescence intensity means distribution. Statistical significance was analyzed through "Two-sample Kolmogorov-Smirnov test" (MATLAB function kstest2) by considering a P-value<0.05 as statistically relevant.

2.6 Immunostaining

Cells were fixed with 4% paraformaldehyde (Sigma-Aldrich) for 7 min at room temperature, permeabilized with 0.5% Triton X-100 (Sigma-Aldrich) and blocked in 10% scomplemented FBS in PBS for 45 min at room temperature. Cells were incubated with primary antibodies against Desmin, rabbit polyclonal (Sigma-Aldrich), myosin heavy chain II, mouse mono-clonal, (Sigma-Aldrich), Dystrophin, mouse monoclonal, (Nova Castra, Buffalo Grove, IL, USA) and Calpain-2 (rabbit polyclonal, Genetex, Irvine, CA) for 1h at room temperature. Cells were washed and incubated with Alexa488 and Alexa495 fluorescence-conjugated secondary antibody (Life Technologies) against mouse or rabbit, depending on primary antibody for 45 min at 37°C. Finally,

nuclei were counterstained with DAPI (Sigma-Aldrich). Samples were mounted with Fluoshield (Sigma-Aldrich) and analyzed through a fluorescence microscope.

2.6 RT-PCR analysis

Total RNA was extracted with TRIzol reagent (Life Technologies) and treated with Turbo DNAfree kit (Applied Biosystems) to remove genomic DNA contamination. First-strand complementary DNA (cDNA) synthesis was performed using an oligo-(dT)20 primer and the cDNA High Capacity cDNA Reverse Transcription Kit (Applied Biosystems). PCR was performed with cDNA using AmpliTaq Gold (Applied Biosystems). Amplifications were performed with an annealing temperature of 62°C for 35 cycles, then amplified fragments were resolved by electrophoresis on a 2% agarose gel, followed by staining with ethidium bromide. Primer sequences were CTGCTGAAGGAGAGGGAGCT (forward) and TGATTAGCTGGTCACACCTT (reverse) for MHC and CCCTTCATTGACCTCAACTACA (forward) and TTGCTGATGATCTTGAGGCTGT (reverse) for GAPDH.

3. Results and discussion

3.1 Stretching device design and fabrication

Cell-stretching device was properly designed in order to ensure: i) accurate control of mechanical stimulations at single-cell level; ii) high temporal resolution of cyclic mechanical stimulations; iii) optical accessibility for in line analysis; iv) statistical significance of treated samples, with internal non-stretched control.

Microfluidic technology, that is recognized to provide highly reproducible and well-defined hydrodynamic conditions, was adopted in order to obtain accurate control of pressure-driven mechanical deformation of elastic membrane underneath cell culture, in terms of amplitude, temporal profile and frequency of cyclic deformation. Pressurization of microfluidic compartment induces mechanical deformation of PDMS membrane and, consequently, of cultured cells (Fig.1A).

In order to reproduce typical *in vivo* muscle fiber strains ranging from 10% to 15% under physiological conditions[35], we developed a Finite Element Model (FEM) of elastic membrane (§2.3) to predict biaxial mechanical deformation and assist microfluidic channel design. We computationally investigated how design parameters, such as PDMS stiffness and membrane geometry, affect membrane deformation to achieve proper mechanical stimulations. Specifically, vertical displacement in the center of the spot, Δh, was predicted for different PDMS stiffness,

namely different prepolymer/curing-agent ratios (5:1, 10:1, 20:1), PDMS membrane thicknesses, *th*, (35, 55, 75 μm) and spot radius values (500, 700, 900 μm). Fig. 1B-D shows *Δh* profile at increasing pressure for different conditions. Extremely deformable membranes can be achieved by increasing prepolymer/curing-agent ratio (Fig. 1B). Similarly, lower membrane thickness promotes higher vertical displacements (Fig. 1C). However, in both cases technical issues due to handling very fragile PDMS layers need to be considered. Higher spot radius increase vertical displacement under pressurization. Larger areas with radius greater than 900 μm enhance possible membrane collapse. Taking into account all these aspects, a PDMS membrane with 10:1 composition, 55 μm thick and with a spot radius of 500 μm was adopted.

Microfluidic network includes 32 independent deformable circular membranes connected through a microfluidic channels network with hydraulic symmetry, which ensures constant pressure drop and identical pressure-induced membrane dynamics, as shown in Fig. 1E (left). The non-stretchable PDMS surface can be used as internal negative control.

Microfluidic cell-stretching device can be easily integrated in standard multi-well plates (Fig. 1E, right) or directly coupled with an optical microscope for in line analysis. This latter solution requires an additional PDMS layer to confine cell culture medium during observation. The experimental set up adopted for stretching experiments is schematically represented in Fig. 1F. Pressurized gas-line and a vacuum apparatus, constantly set at 0.8 bar, are connected to a set of micro-valves, which are alternatively open to pressure or vacuum. An external electronic device automatically regulates micro-valves switch through Labview software, which allow controlling cyclic mechanical stretch frequency.

3.2 Cell stretching device validation

Thanks to microscopic dimensions of microfluidic channels, few microliters holdup (100 nL for single spot and 2.4 uL for the whole network) and extremely low liquid handling are required to achieve system pressurization, thus providing fast dynamics of the stimulation and uniform spatial and temporal stimulus of cultured cells.

Fig. 2A shows the overall spot deformation in both radial and circumferential direction, obtained by FEM analysis. We experimentally validated the derived model by measuring vertical displacements (as reported in §2.3) at increasing pressures and comparing experimental values with the predicted ones. Theoretical profile, obtained by numerical solution, resulted in good agreement with the experimental values (Fig. 2B), thus confirming the robustness of the derived model.

Fig. 2C shows radial and circumferential strain profile along *r*-coordinate for different pressure

intensities, i.e. 1 and 0.25 bar. Based on these data, further analysis of cell stretching will be confined to a smaller area of the spot, namely a concentric circle of 300 μm radius, in order to minimize strain variations. A pressure intensity of at least 1 bar were used in order to ensure at least 10% strain, which is consistent with deformation of muscle fiber *in vivo*.

In order to assess the robustness of our system and the reproducibility of mechanical stimuli during cyclic deformations, microfluidic channels were filled with a dye solution to detect the absorbance of deformed areas during pressurization cycles, at different frequency. These values of absorbance were directly correlated to the vertical displacement of the membrane. Fig. 2D shows temporal profiles of absorbance acquired at different frequencies ranging from 0.1 to 1 Hz and demonstrates the efficiency of the system in terms of stability of the mechanical deformation and fast dynamics. Fig. 2E shows areal strain dynamics; 90% of the maximum deformation were obtained in 0.2 s, confirming the high temporal resolution that could be achieved using microfluidic setup to over-impose high frequency cyclic mechanical stimulations.

In order to verify whether the developed device could induce a biological response on a cell culture under cyclic stimulation, we subjected a C2C12 myoblasts to both static and cyclic (1 Hz) mechanical stretch for 2 h. Analysis of cyclically stretched cells resulted in a remodeling of cytoskeletal actin filaments, confirmed by stress fibers alignment along the direction of minimum strain, i.e. the circumferential direction (Fig. 3). The same result was not observed by applying a static deformation. These experimental observations provide evidence of a frequency-dependent cytoskeletal remodeling in response to mechanical stimulations, consistently with data reported in the literature[30],[34].

3.3 Cyclic mechanical stretch affects dystrophic myotubes membrane integrity

We next investigated whether lacking of Dystrophin, which is recognized to preserve membrane structure and homeostasis in human skeletal muscle, is associated with membrane damages induced by cyclic mechanical stress. Specifically, we investigated whether cyclic mechanical stimulation affects membrane integrity in a human DMD *in vitro* model by subjecting human healthy and DMD myotubes to a series of 15% physiological strains at 0.5 Hz.

To this purpose, microfluidic cell-stretching devices were properly functionalized as previously described, in order to achieve long-term cell attachment during myoblasts differentiation. Purity of myoblasts populations, derived from biopsies of healthy donors and DMD patients, was assessed by immunofluorescence analysis of the early myogenic marker DESMIN (Fig. 4A).

Myoblasts were seeded and induced to differentiate into fused myotubes when reaching 90% confluence (Day 0) for other 6 days. We first verified the two cell populations followed the same

differentiation pattern on PDMS substrates by RT-PCR analysis of the late myogenic marker myosin heavy chain (MHC), which showed increasing level of expression for both healthy and DMD samples (Fig. 4B). At protein level, multinucleated myotubes at Day 6 of differentiation were positive for MHC, also showing well-organized sarcomeric striations in both healthy and DMD cells. DYSTROPHIN expression with membrane localization was observed in myotubes derived from healthy individuals, whereas DMD myotubes resulted DYSTROPHIN-negative, confirming the diseased phenotype (Fig. 4C). All together these results show that proper human myoblast differentiation was achieved even on non-conventional substrates, like PDMS surface.

In order to validate the hypothesis that membrane integrity could be affected by prolonged cyclic mechanical stimulations in DMD condition, we developed a functional assay in which membrane permeability to large molecules, induced by mechanical stresses, was analyzed through the use of a membrane impermeant fluorescent marker. Human myotubes were loaded with 4 µM FM 1-43 membrane impermeant marker and cyclically stretched for a defined timespan at 0.5 Hz, as shown in the Supplementary Video 1.

Over-physiological stimulation above 20% strain was induced in healthy human myotubes by increasing pressure from 1 to 2 bar, leading to widespread fluorescent signal in myotubes confined within the stretching area, due to loss of membrane integrity (Fig. 4D). The results showed that only the myotubes exposed to mechanical stimulation displayed marked internal membrane, confirming that the non-stimulated regions of the device could be used as internal control for the experiments.

The stretching assay was also performed in physiologic condition (15% strain) with both healthy undifferentiated myoblasts and differentiated myotubes following FM 1-43 uptake in a timespan of 30 min (Fig. 4E). Interestingly, only stretched myotubes and not myoblasts display an increasing fluorescent signal at the last time-point. We observed high viability of FM 1-43-positive myotubes after 24 h (Live&Dead assay, data not shown). According to these observations we concluded that the stress-induced membrane permeability could be a transient and reversible phenomenon that do not cause short-term cell death.

In order to validate the hypothesis proposed that cyclic mechanical stimulations could differentially affect the membrane integrity in healthy and DMD myotubes, we performed different cyclic stimulations under physiological stress conditions for two time intervals, i.e. 90 and 45 min.

Taking advantage of having an internal non-stretched control we analyzed fluorescence intensity of stretched and control myotubes in the same conditions and with the same fluorescence background. Fluorescence intensity in the cytosolic regions of myotubes was quantified as described in §2.5 and results were represented as intensity means distribution of region of interests, ROIs (N=96), as shown in Fig. 5A-B.

Fig. 5B shows a not significant difference in fluorescence intensity distributions of control and stretched myotubes derived from healthy individuals (P-value=0.973). On the other hand, fluorescence intensity distributions of dystrophic myotubes show a significant difference between stretched and control cells (P-value=0.029).

These results demonstrate that lack of Dystrophin strongly affects membrane integrity of human myotubes when subjected to cyclic mechanical stretch. Stimulations longer than 90 min were not taken into account for possible cell detachment during stretch cycles.

We further investigated whether stretch-induced membrane permeability increase in dystrophic myotubes for a shorter period of cyclic stretch (45 min at 0.5 Hz and 15% strain, Fig. 5C). Quantification of fluorescence intensity confirmed a not significant difference between the two distributions, meaning that permeability increase appears in a later temporal interval (Fig. 5D) and confirming that long term stimulation is required to compromise membrane integrity in DMD myotubes.

These experimental evidences validates the hypothesis reported in literature, that the absence of Dystrophin makes the membrane more fragile and more susceptible to mechanical stress leading to increased membrane permeability[18]. Many studies recognize, as consequence, abnormal cytosolic calcium concentrations in DMD muscle fibers compared to healthy ones. This higher intracellular calcium level is also known to contribute to muscle degeneration through the aberrant activation of calcium dependent proteases, Calpain-1 and Calpain-2[36]. The implication of Calpains in disorders such as dystrophies has identified them as important potential therapeutic targets and has raised interest in the use of specific Calpain inhibitors as a potent treatment[37,38]. Observation of a four-fold increase in muscle Calpain-2 mRNA levels in muscle fibers from DMD patients, compared to control, confirms enhanced expression of the Calpain-2 gene in dystrophic condition, explaining the enhanced activity of the enzyme, and highlights its importance in DMD pathogenesis[39].

We therefore verified the role of cyclic stretch in affecting Calpain-2 expression in dystrophic myotubes compared to the healthy ones by immunofluorescence analysis. Fig. 6A shows immunofluorescence analysis of Calpain-2 in myotubes derived from healthy individual and DMD patient. Interestingly, we observed a different Calpain-2 localization for the two controls; healthy myotubes displayed well-defined nuclear signal, whereas DMD myotubes showed cytosolic staining. After exposing myotubes to 90 min 15% cyclic deformation at 0.5 Hz, we observed cytosolic localization of Calpain-2 for both healthy and DMD myotubes (Fig. 6B). These results suggested that only healthy myotubes show Calpain-2 alteration compared to the control, probably due to a transient physiological increase of intracellular calcium during mechanical stimulation[18]. On the other hand, DMD myotubes show no significant difference in Calpain-2 staining, consistent

with the higher level of calcium and Calpain-2 basal activity, normally reported in DMD muscle. Further experiments will be required to rationally dissect the role of membrane integrity, intracellular calcium level and Calpain-2 activity in early stage of DMD pathogenesis.

4. Conclusions

In conclusion, we investigated the role of cyclic mechanical stretch in a human DMD *in vitro* model, by developing an *ad hoc* microfluidic-based cell-stretching device. We first demonstrated that the developed device could be used to obtain a biological response on a cell culture, by showing a frequency-dependent cytoskeletal remodeling of stress fibers after a cyclic mechanical stimulation. We then focused on the role of cyclic stretch in affecting membrane permeability increase of dystrophic myotubes compared to the healthy ones. Stretch-induced membrane permeability results to increase in a temporal window from 45 to 90 min. This susceptibility of membrane integrity could be associated to slow accumulation of intracellular calcium, which results already altered activation of calcium-dependent protease Calpain-2 in DMD myotubes.

More generally, the developed approach could be successfully used to investigate early pathologic events on human dystrophic muscle tissue caused by mechanical stresses that mimic those at which the muscle fibers are exposed *in vivo*.

Acknowledgments

Bibliography

1 A. Salameh, A. Wustmann, S. Karl, K. Blanke, D. Apel, D. Rojas-Gomez, H. Franke, F. W. Mohr, J. Janousek and S. Dhein, *Circulation Research*, 2010, **106**, 1592–1602.

2 A. Kumar, *The FASEB Journal*, 2004, **18**, 1524–1535.

3 S.-H. Kook, H.-J. Lee, W.-T. Chung, I.-H. Hwang, S.-A. Lee, B.-S. Kim and J.-C. Lee, *Mol. Cells*, 2008, **25**, 479–486.

4 S. Suresh Babu, A. Wojtowicz, M. Freichel, L. Birnbaumer, M. Hecker and M. Cattaruzza, *Sci. Signal.*, 2012, **5**, ra91.

5 H.-J. Hsu, C.-F. Lee, A. Locke, S. Q. Vanderzyl and R. Kaunas, *PLoS ONE*, 2010, **5**, e12470.

6 P. G. De Deyne, *American Journal of Physiology-Cell Physiology*, 2000, **279**, C1801–C1811.

7 F. Rahimov and L. M. Kunkel, *J Cell Biol*, 2013, **201**, 499–510.

8 E. M. McNally and P. Pytel, *Annual Review of Pathology: Mechanisms of Disease*, 2007, **2**, 87–109.

9 D. J. Blake, A. Weir, S. E. Newey and K. E. Davies, *Physiol Rev*, 2002, **82**, 291–329.

10 E. W. Yeung, N. P. Whitehead, T. M. Suchyna, P. A. Gottlieb, F. Sachs and D. G. Allen, *J Physiol*, 2005, **562**, 367–380.

11 R. J. Khairallah, G. Shi, F. Sbrana, B. L. Prosser, C. Borroto, M. J. Mazaitis, E. P. Hoffman, A. Mahurkar, F. Sachs, Y. Sun, Y.-W. Chen, R. Raiteri, W. J. Lederer, S. G. Dorsey and C. W. Ward, *Sci. Signal.*, 2012, **5**, ra56.

12 A. Kumar, *The FASEB Journal*, 2004, **18**, 102–113.

13 C. Y. Matsumura, A. P. T. Taniguti, A. Pertille, H. S. Neto and M. J. Marques, *Am J Physiol Cell Physiol*, 2011, **301**, C1344–C1350.

14 C. Mann, E. Perdiguero, Y. Kharraz, S. Aguilar, P. Pessina, A. Serrano and P. Muñoz-Cánoves, *Skeletal Muscle*, 2011, **1**, 21.

15 T. M. Suchyna and F. Sachs, *The Journal of Physiology*, 2007, **581**, 369–387.

16 D. G. Allen and N. P. Whitehead, *The International Journal of Biochemistry & Cell Biology*, 2011, **43**, 290–294.

17 Allen DG, Gervasio OL, Yeung EW and Whitehead NP, *Canadian journal of physiology and pharmacology*, 2010, **88**, 83–91.

18 D. G. Allen and N. P. Whitehead, *The International Journal of Biochemistry & Cell Biology*, 2011, **43**, 290–294.

19 B.-T. Zhang, N. P. Whitehead, O. L. Gervasio, T. F. Reardon, M. Vale, D. Fatkin, A. Dietrich, E. W. Yeung and D. G. Allen, *J Appl Physiol*, 2012, **112**, 2077–2086.

20 P. W. Hamer, J. M. McGeachie, M. J. Davies and M. D. Grounds, *Journal of Anatomy*, 2002, **200**, 69–79.

21 E. W. Yeung and D. G. Allen, *Clinical and experimental pharmacology and physiology*, 2004, **31**, 551–556.

22 X. Trepat, L. Deng, S. S. An, D. Navajas, D. J. Tschumperlin, W. T. Gerthoffer, J. P. Butler and J. J. Fredberg, *Nature*, 2007, **447**, 592–595.

23 A. Grossi, A. H. Karlsson and M. A. Lawson, *Cell Biology International*, 2008, **32**, 615–622.

24 S. Akbari and H. R. Shea, *J. Micromech. Microeng.*, 2012, **22**, 045020.

25 R. J. Khairallah, G. Shi, F. Sbrana, B. L. Prosser, C. Borroto, M. J. Mazaitis, E. P. Hoffman, A. Mahurkar, F. Sachs, Y. Sun, Y.-W. Chen, R. Raiteri, W. J. Lederer, S. G. Dorsey and C. W. Ward, *Sci. Signal.*, 2012, **5**, ra56.

26 B. L. Prosser, R. J. Khairallah, A. P. Ziman, C. W. Ward and W. J. Lederer, *Journal of Molecular and Cellular Cardiology*, 2013, **58**, 172–181.

27   Q. Wang, X. Zhang and Y. Zhao, *Journal of Micromechanics and Microengineering*, 2013, **23**, 015002.

28   Q. Wang, X. Zhang and Y. Zhao, *Sensors and Actuators B: Chemical*, 2014, **194**, 484–491.

29

30   C. S. Simmons, J. Y. Sim, P. Baechtold, A. Gonzalez, C. Chung, N. Borghi and B. L. Pruitt, *J Micromech Microeng*, 2011, **21**, 054016–054025.

31   C. Moraes, M. Likhitpanichkul, C. J. Lam, B. M. Beca, Y. Sun and C. A. Simmons, *Integr. Biol.*, 2013, **5**, 673–680.

32   C. Moraes, J.-H. Chen, Y. Sun and C. A. Simmons, *Lab Chip*, 2010, **10**, 227–234.

33   J. Zhou and L. E. Niklason, *Integr Biol (Camb)*, 2012, **4**.

34   D. Tremblay, S. Chagnon-Lessard, M. Mirzaei, A. E. Pelling and M. Godin, *Biotechnol Lett*, 2014, **36**, 657–665.

35   C. C. van Donkelaar, P. J. Willems, A. M. Muijtjens and M. R. Drost, *J Biomech*, 1999, **32**, 755–762.

36   B.-T. Zhang, S. S. Yeung, D. G. Allen, L. Qin and E. W. Yeung, *Journal of Applied Physiology*, 2008, **105**, 352–357.

37   M. Bartoli, N. Bourg, D. Stockholm, F. Raynaud, A. Delevacque, Y. Han, P. Borel, K. Seddik, N. Armande and I. Richard, *J. Biol. Chem.*, 2006, **281**, 39672–39680.

38   N. P. Whitehead, M. Streamer, L. I. Lusambili, F. Sachs and D. G. Allen, *Neuromuscular Disorders*, 2006, **16**, 845–854.

39   T. Hussain, H. Mangath, C. Sundaram and M. Anandaraj, *Journal of Genetics*, 2000, **79**, 77–80.

Figure captions

Figure 1. **Microfluidic cell stretching device**. (A) Cross-section view of a single stretching unit. Pressurization of the microfluidic compartment (ΔP>0) induces PDMS membrane deformation and, consequently, mechanical stimulation of cultured cells. *Th* indicates membrane thickness above the microfluidic channel, whereas Δh is the vertical displacement of the membrane in the correspondence of the axial of symmetry. (B-D) Heat maps of membrane deformation at defined pressure based on FEM analysis (ΔP=1bar) (up). Vertical displacement profile at increasing pressures (down). Different PDMS stiffness (B), thickness (C) and geometries (D) were considered. (E) Top view of the microfluidic network composed by 32 different spots with 1mm diameter (left) and integration of the microfluidic cell-stretching device within a standard 6-well plate (right). (F) Experimental set up. Mechanical stretch in the microfluidic device is controlled through a series of micro-valves continuously switching through pressurized air-line and vacuum, constantly set at 0.8 bar. An external electronic device automatically regulates micro-valves switch through Labview software, controlling stretch frequency. Blue line indicates the interface between gas phase and liquid used to prevent oxidative stress to the cells.

Figure 2. **Characterization of cyclic deformation.** (A) 3D-view of spot strain at defined pressure (ΔP=1bar) in radial and circumferential direction based on FEM analysis. (B) Comparison of Δh experimental values and the predicted profile derived through FEM analysis as a function of the applied pressure. (C) Strain profile in radial (black) and circumferential (red) direction along *r*-coordinate at different pressure. In the graph is also shown the area of interest for membrane integrity analysis. (D) Temporal profile of the mechanical stimulus at different frequencies, obtained by filling microfluidic channels with a dye and recording the absorbance in the center of the membrane at different frequencies. This value of absorbance is directly correlated to the vertical displacement of the membrane and to the cell adhesion surface deformation. (E) Absorbance values were converted in surface deformation values, in order to evaluate the dynamic of mechanical stimulation along *r*-coordinate.

Figure 3. **Stretch frequency-dependent cytoskeletal remodeling in C2C12 myoblasts.** Bright field and F-actin staining pictures of C2C12 myoblasts non-stretched, statically stretched for 2h (0 Hz, 12 %
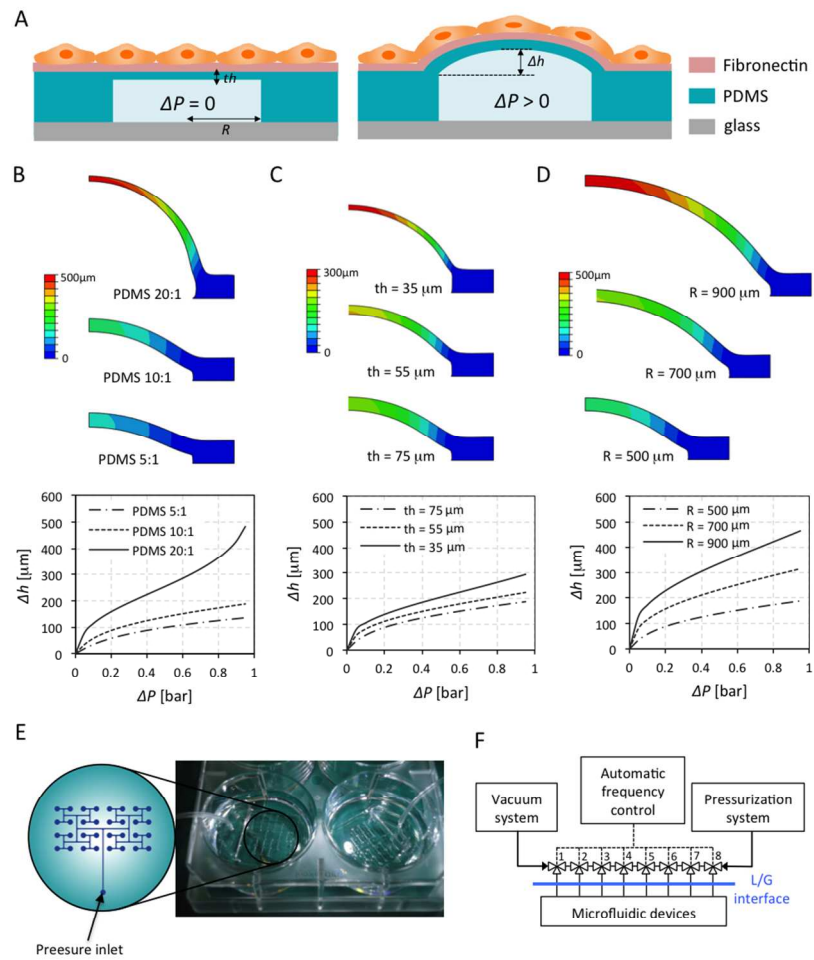
strain) and cyclically stretched for 2h (1 Hz, 12 % strain). In the last case a cytoskeletal remodeling perpendicular to the direction of maximum strain, i.e. radial direction, was observed.

Figure 4. **Development of a membrane-integrity assay in a human DMD *in vitro* model.** (A) Immunofluorescence analysis of early myogenic marker DESMIN in healthy and DMD myoblasts showing cell population purity. (B) RT-PCR analysis of MHC expression during myoblasts differentiation in stretching devices. GAPDH was used as reference gene. (C) Immunofluorescence analysis of MHC and DYSTROPHIN expression at Day 6 of differentiation in healthy and DMD myotubes. Both healthy and DMD myotubes display homogeneous MHC expression with well-defined sarcomeric organization. DYSTROPHIN expression was detected only in healthy myotubes, with membrane localization. (D) Stretching region-confined dye uptake in myotubes exposed to 20% (non-physiologic) static strain. (E) Time-course of FM 1-43 dye uptake in myoblasts at Day 1 compared to myotubes at Day 6. Only stretched myotubes and not myoblasts display a slight marker uptake with an increasing fluorescent signal.

Figure 5. **Stretch-induced membrane permeability analysis in DMD compared to healthy myotubes.** (A) Representative images of FM 1-43 dye uptake in healthy and dystrophic myotubes after 90 min cyclic stretch (0.5 Hz, 15% strain) compared to non-stimulated control myotubes. (B) Fluorescence intensity distribution of stretched healthy myotubes is not statistically different from the non-stretched control. Fluorescence intensity distribution of stretched DMD myotubes result statistically different from the un-stretched control. (C) Representative images of FM 1-43 dye uptake in dystrophic myotubes after 45 min cyclic stretch (0.5 Hz, 15% strain), compared to non-stretched control myotubes. (D) Fluorescence intensity distribution of stretched myotubes is not statistically different from the non-stretched control. (*n*=3)
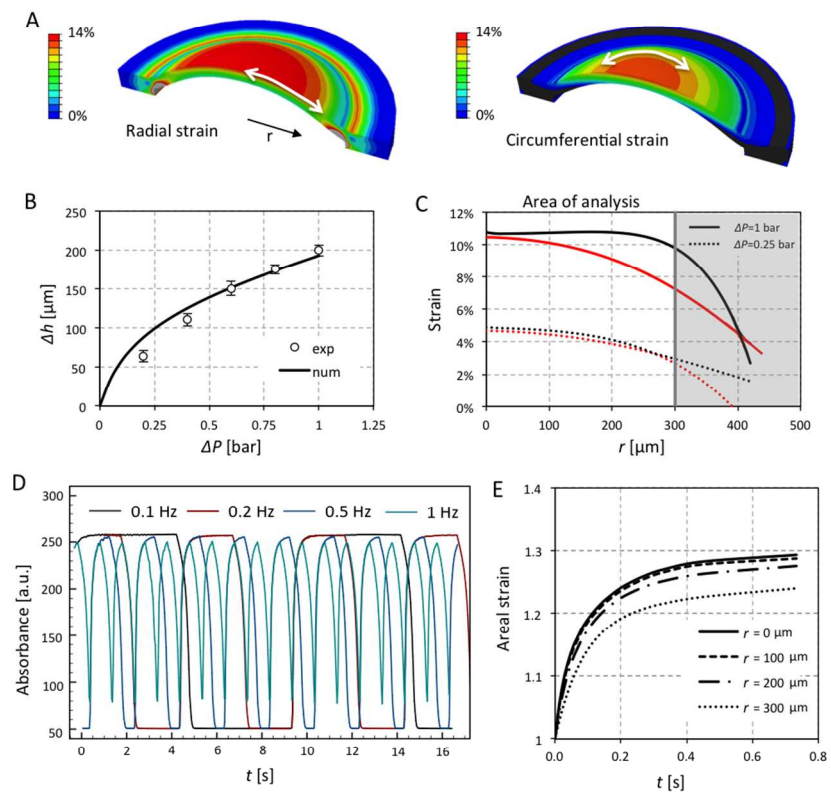
Figure 6. **CALPAIN-2 expression in healthy and DMD myotubes.** (A) Immunofluorescence analysis of calcium-dependent protease CALPAIN-2 expression in myotubes. (B) Immunofluorescence analysis of CALPAIN-2 expression in healthy and DMD myotubes exposed to 90 min 15% cyclic strain at 0.5 Hz.
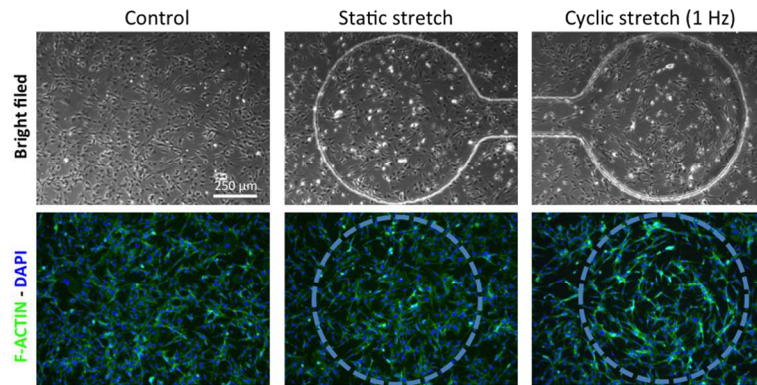
Figure 1

A

B

C

D

PDMS 20:1

PDMS 10:1

PDMS 5:1

th = 35 µm

th = 55 µm

th = 75 µm

R = 900 µm

R = 700 µm

R = 500 µm

E

F

Preesure inlet

352x509mm (72 x 72 DPI)

Figure 2

Figure 3

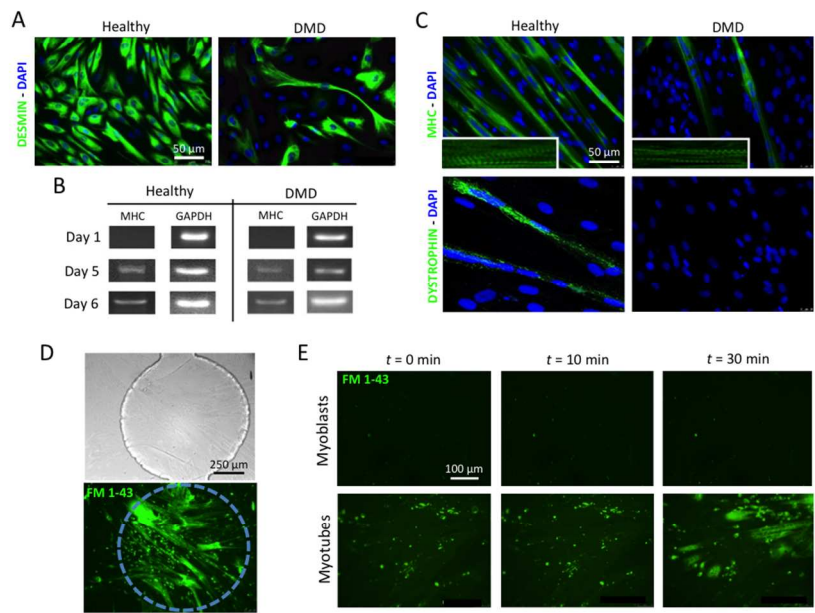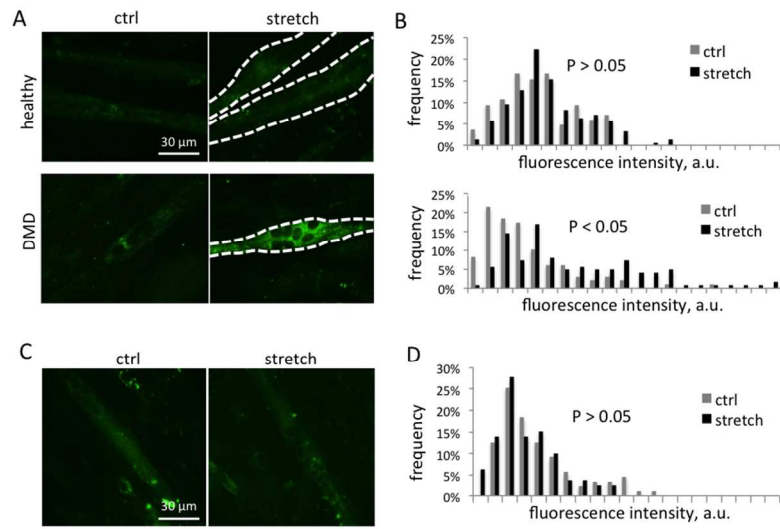

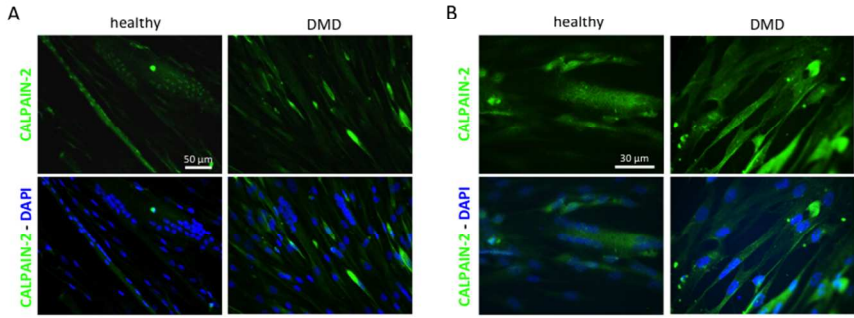352x509mm (72 x 72 DPI)

Figure 4

352x509mm (72 x 72 DPI)

Figure 5

352x509mm (72 x 72 DPI)

Figure 6

352x264mm (72 x 72 DPI)